

Visual and semi-automated interpretation methods for urban flood detection using SAR Sentinel-1A image: study case in North Aceh Regency, Indonesia

Ayyasy Muhammad Fadhil¹ and Akhyar^{2*}

1. Department of Earth Technology and Science, Universitas Syiah Kuala, Banda Aceh, 23111, INDONESIA

2. Department of Mechanical Engineering, Universitas Syiah Kuala, Banda Aceh, 23111, INDONESIA

*akhyar@unsyiah.ac.id

Abstract

Flood is a natural disaster when causes damage and loss, especially in urban areas that are inhabited by many people and have many properties. The goal of this study is to map rapidly the flooded areas in North Aceh district on January, 5 2022 using multi-temporal SAR Sentinel-1A images through visual interpretation and semi-automated interpretation methods including thresholding and support vector machine (SVM). Visual interpretation relied on multi-polarization image of VH-VV with median filters of 3x3 and 5x5.

This study produced the flooded area maps from three methods used with an area of each method: visual interpretation (422.86 ha), thresholding (791.22 ha) and SVM (1084.76 ha). According to the comparison with the result generated from visual interpretation using Planetscope-3A, SVM method has the similar result in the flooded areas with an area of 1001.52 ha. This study also analysed impact of flood event against land cover referring to Sentinel-2 10-Meter Land Use/Land Cover of ESRI and showed that class of cultivated crops is most affected. Results show that this study can be very helpful in damage and loss assessment of flood event and can be reference for urban planning management in order to face the climate change.

Keywords: Flood, Sentinel-1A, Visual interpretation, Support Vector Machine, Thresholding, Planetscope-3A.

Introduction

Flood is an overflow or inundation that comes from a river or other body of water on the ground because of long-lasting rainfall^{3,26} and it becomes disaster when causes damage and loss to lives, infrastructures and environments.^{18,21} It happens when people live in “wrong” condition and ways such as the excessive urbanization²⁵ and the factors of logging, paving and building construction so that soil and vegetation are difficult to absorb the water from downpours.^{27,51} Floods occurring in urban areas result in the big impact of economic loss and injuries in community.³⁷ Understanding the flood mitigation is essential for disaster risk reduction before and after events utilizing active remote sensing for floods mapping.²² Flood can be classified as the quick and sudden disaster types but are among few in this

category that can be well predicted, anticipated and controlled to a great extent.²¹ The rapid needs for flood mitigation require us to take advantage of radar satellite that can adapt to rapid flood events and conditions at the location. Mapping of flooded areas produces a historical sources-based data that is useful for natural disaster assessment highlighted to the occurrence rate, duration and spatial extent.²⁰

Radar satellite records the earth by using microwave energy that has the advantages: able to penetrate atmosphere in all weathers, especially in rainy season.³¹

It provides the opportunity for development of radar remote sensing in observing large parts of Earth’s land including flood observation.⁴ Sentinel-1A satellite is the best data source for floods mapping because its synthetic aperture radar (SAR) sensor produces the images once in 6–12 days. SAR sensor has been a valuable means for hydrological assessment for the three decades.¹⁷ The availability of these close time series images with its complex coherence constitutes an advantage from at least two points of view: allows to infer precious information about the nature and genesis of the recurrent floods and prevents the main errors consisting of spatial and temporal decorrelations.⁶

SAR Sentinel-1A sensors have the high potential to detect flood extents in urban areas because their amplitude enables the easy identification by distinguishing the land and water or water bodies contrast.^{1,15,34,45} Change detection of flood is good to perform using multi-temporal SAR images of pre-flooding and flooding in order to mask out permanent water bodies and flood water.⁵⁰ Scattering of bare soil gets decreased and also reduces factor resisting coherence which microwave will interact directly to water surface with specular reflection alongside vegetated areas and urban areas.

Flooded areas have the low intensity because the water surface roles as specular reflector, causing water bodies look as darker or black tone. Change detection method is effective for rapid monitoring against the abrupt change to the land surface in order to derive pattern of change caused by flood.^{36,52}

The difficulties of finding an adequate image in the archive and of correctly interpreting all detected changes in backscatter represent the main limitations of flooding-related change detection.¹² Analysis of images obtained in

non-flood condition is useful to distinguish permanent and transient water bodies and to accurately delineate the floodwaters on any given day.^{12,44}

Flood detection can be done through visual interpretation method based on characteristics of earth surface terrain that can show condition of environment in an area using several variation of SAR image processing to generate the best image visual appearance. Important information in image can be extracted through multi-polarization utilizing different image polarization types.¹¹ Multi-polarization system can enhance radar capabilities in monitoring and identifying objects on earth's surface.^{23,29}

Threshold-based methods also can be used for flood detection in order to obtain the best appearance by separating the water and high land pixels.³⁴ An adaptive threshold is essential for change detection to map the flooded bare soils and flooded built-up areas.⁵ Results of flood mapping with homogeneous land surfaces using threshold are quite sensitive to the chosen threshold values.⁵⁰ Besides the quality of change image, the quality of the thresholding highly affects the overall performance of change detection.²⁸

Another method that can be used to detect floods is supervised classification. Support Vector Machine (SVM) is one of the new generation learning systems based on recent advances in statistical learning theory delivering State of the Art performance in real-world application.¹⁰ SVM has been widely used for land cover classification but not much for flood study. SVM method has been carried out in several studies for flood prediction analysis by distinguishing

flooded and non-flooded areas.^{24,46,49} SVM in flooded area classification can generate a hyperplane of water level change on the basis of the rising in water level at flood event.⁴⁹

The purpose of this study is to map the flooded area with case study of flooding in North Aceh, 5 January 2022, using methods of visual interpretation and semi-automated interpretation including thresholding and SVM.

The benefits of this study are to find out the best method to map the flood quickly in urban area through radar image to know the flood-prone areas and can be used as a tool in supporting the flood mitigation plan management. Identification of flood prone areas is useful to communicate flood disaster information to concern authority as well as to the people.⁸

Material and Methods

Study area: In early 2022, most of the North Aceh area experienced the devastating flood event from 1 January 2022 to 7 January 2022 caused by high rain frequency and the rising river level over several days. This flood event caused damage and loss of infrastructures and victim especially in urban area.

This study focused in urban area of North Aceh, Aceh Province with an area of 80.01 km² (96°57'28.7" E 5°15'39.8" N–97°2'49.0" E 5°10'55.7" N). The study area has the average height of 26 meters above sea level (85 feet) (Figure 1).

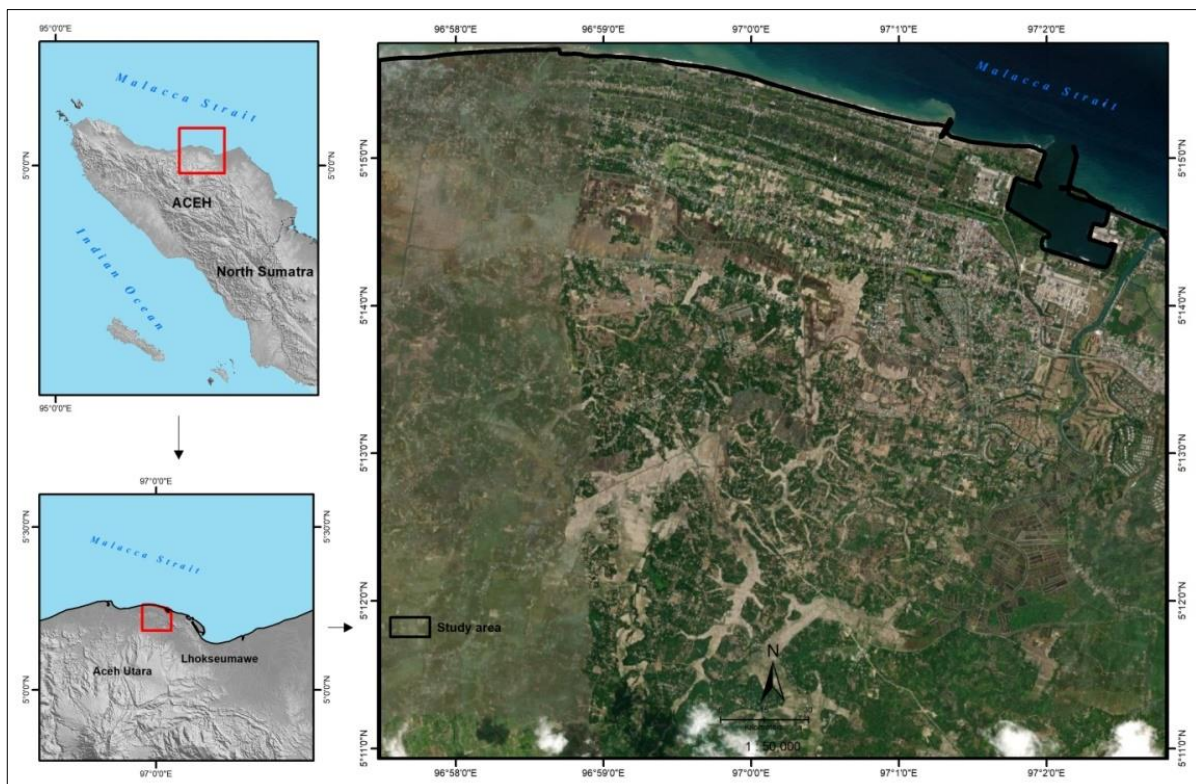


Figure 1: Study area

Data: Data used for this study are multi-temporal SAR Sentinel-1A images. To select an adequate reference image, images should have been acquired during the same season as the flood image, especially for applications in regions characterized by a pronounced seasonality in moisture and vegetation growth.¹² Image of study area inundated by flood was captured by Sentinel-1A satellite with recording time of 5 January 2022 and Sentinel-1A images on periods of pre-flooding acquired from Copernicus Open Access Hub of ESA’s Sentinel missions were also used with recording time of 14 August 2021. The ancillary image used is high resolution image Planetscope-3A acquired from Planet missions. Land cover used for this analysis is Sentinel-2 10-Meter Land Use/Land Cover of ESRI. Table 1 shows the details about the images used.

Methodology

Image processing: The main image processing steps began from calibration, speckle filtering and geometric correction. All these steps were included in multi-temporal image analysis techniques.¹³ These operations steps are typically performed to improve the overall accuracy.² Calibration has

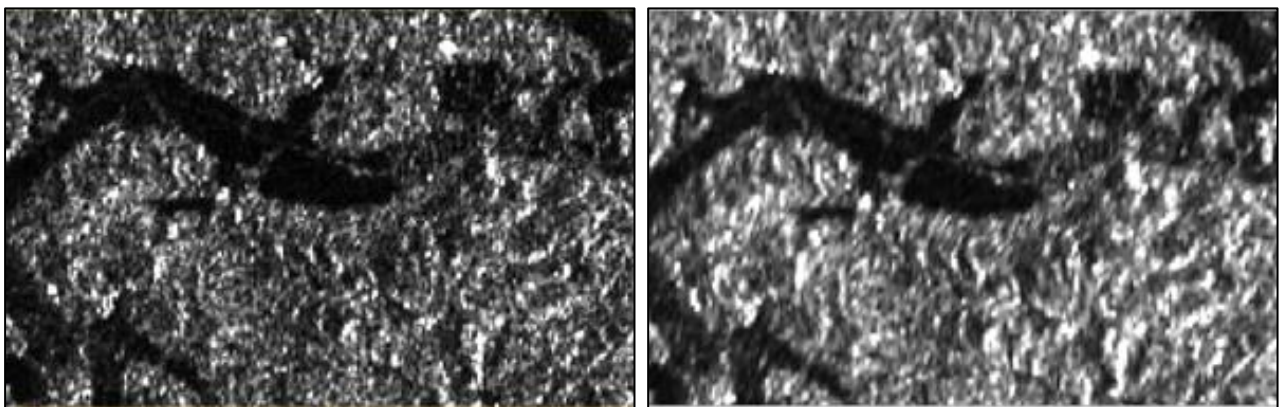
the function to provide imagery in which the pixel value can be directly related to the radar backscatter of the scene.¹⁶ Speckle noise in SAR images caused the degradation of the quality of the image and the difficulty of feature interpretation.¹⁶ It can be reduced either by spatial filtering or multi-looking processing to enhance the appearance contrast and improve the results of subsequent phases.¹³

Geometric correction is intended to compensate variations of topographical distortion in order to make geometric representation of image as close as possible to the real world. It is able to solve the ambiguity and to discriminate these two features (water body and radar shadows).⁴⁸ Figure 2(a) and 3(b) images were generated from multi-looking by converting from slant range to ground range using number of range and azimuth looks of 1x3 and 2x4.

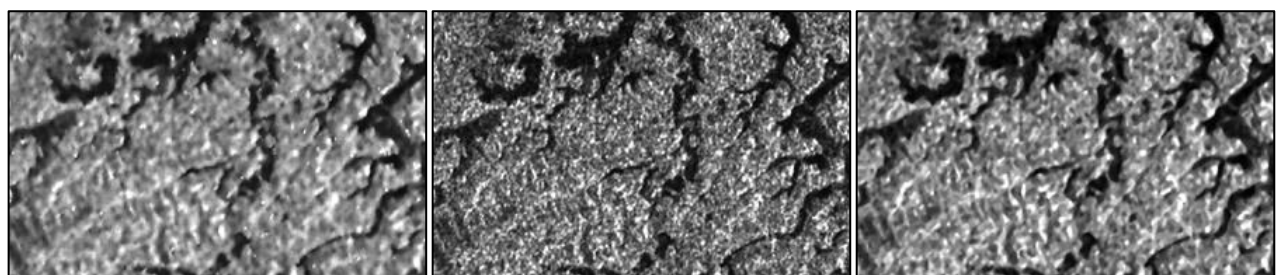
Image in figure 2(a) provides the rougher display on land surface and strong natural black colour on water. Image in figure 2(b) provides the smoother display with less speckles on land surface, however provides more blur display on water due to the reduction of excessive pixel value between number of range and azimuth looks.

Table 1
Data used in this study for flooded area mapping

Data	Spatial resolution	Sensing time	Track / Orbit	Product level / Type
Sentinel-1A	5 x 20 m	14-08-2021 / 23:20:01	135 / 41332	L1 / SLC
		05-01-2022 / 23:20:01	135 / 39232	L1 / SLC
DEM SRTM	30 m	-	-	-
ESRI land cover	10 m	-	-	-
Planetscope	3 m	07-01-2021 / 03:33:07	1025	3A / PS2



(a) (b)
Figure 2: Images generated from multi-looking process



(a) (b) (c)
Figure 3: Images generated from speckle filtering process

It affects the performance in visual interpretation that is purely based on the applicability and the visual appearance of image. Image in range and azimuth of 1x3 still maintain information of water. Figure 3 shows images generated from speckle filtering and kernels of Lee sigma 7x7, Median 3x3 and Median 5x5.

Images generated from three speckle filtering methods (Figure 3) were assessed qualitatively. Lee Sigma 7x7 (Figure 3a) reduces a lot of speckles and provides the smooth display of image, but creates a lot of disturbances that covers water information. Median 3x3 (Figure 3) provides the sharper tones on water with the strong black colour. Median 5x5 (Figure 3) provides clear appearance on water body and removes most of speckles on surface land and water. Therefore, new images generated from combination of median filter with kernel of 3x3 and 5x5 were used as data of multipolarization method for visual interpretation.

Multi-polarization is method of using multiple polarimetric returns to infer information of surface including vegetation and hydrology.³⁸ Multi-polarization provides additional detail about surface features through the different and complementary echoes. It comes from dual polarization Level-1 Single Look Complex (SLC) products which contain complex values.¹⁶ By varying the polarization of transmitted signal and receiving several different polarized images from the same series of pulses, it can produce detailed information of observed surface.

Flood detection: Flood detection in this study was conducted by change detection method to reduce the misclassifications.¹⁹ Flood detection by identifying of water in SAR image refers to the characteristics of low radiometric values.³ Intensity and coherence characteristics of flood water in COSMO-SkyMed and TerraSAR-X images for each case studies had the lower coherence than non-flooded ones.^{7,41} Both of these are required to produce an accurate inundation map in urban areas.³⁰

This study used visual interpretation and semi-automated interpretation methods including thresholding and SVM.

Flood detection using remote sensing image is better to do through both visual and digital interpretation because they associate spectral signature each other with different land covers. The grey tones ranging from black to white of radar image are very helpful to interpret the flooded and non-flooded areas.¹⁵

Visual interpretation method for flood detection was done by delineating the flood prone areas producing the accurate and precise result.⁷ A simple visual interpretation consists of identifying changes between a pair of multi-temporal images through a simple color composition, allowing qualitative identification of flooded and non-flooded areas.^{13,33} Visual delineation was done using coherence value of pixel to distinguish flood with other land cover in urban area; flooded urban area has low coherence value and non-flooded urban area has high coherence value^{7,35} and colour difference. Color composition in SAR image can be generated utilizing its polarization variations by multi-polarization method.

This method is the need for rapid flood mapping after event because it is computationally efficient in fast visualization. Thresholding method consists of assigning to the semantic class “flooded” all pixels with a backscattering value lower than a given threshold.¹² This method was conducted by selecting a threshold value to distinguish between water and non-water. This value is determined by analysing the pixel values indicated as flooded area in a histogram. The choice of threshold depends on environmental and system parameters (frequency band, polarization and observation angle).¹³

Determination of threshold value in pre-flooding period referred to the result of permanent water body classification to prevent the misclassification of flood water value. The availability of pre-flooding and flooding images can generate the color composition difference of flooded and non-flooded areas and can show the change patterns in RGB association (R=image of difference between pre-flooding and flooding; G and B=flooding image).

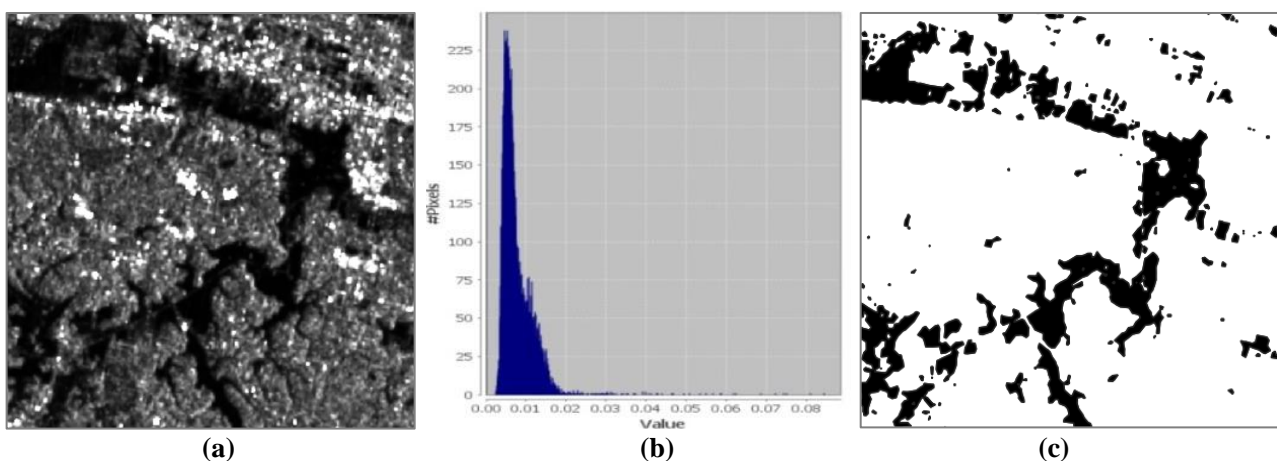


Figure 4: Thresholding process

It will be helpful to show the temporarily inundated areas^{13,14} and it will enhance the change effect in images and increases the interpretability.⁴⁰ Figure 4 presents the scheme of thresholding process.

Figure 4 presents the histogram generated from VH polarized image (Figure 4a) indicating that the pixel values of flooded area are at a range of 0.00 – 0.32 (Figure 4b). Figure 4(c) presents the result of flood water extraction generated from thresholding. Another digital interpretation method used in this study is Support Vector Machine (SVM).

SVM is particularly appealing in the remote sensing field due to its ability in generalizing well with limited training samples.³⁹ SVM is a non-parametric statistical learning algorithm aimed at binary classification by defining optimal hyperplane providing maximum margin separating two classes without assumption made on the underlying data distribution.⁴⁷ The aim of SVM is to find a hyperplane that separates the dataset into a discrete predefined number of

classes in a fashion consistent with the training examples.^{9,39} Figure 5 shows the illustration of scenario in SVM.

Training samples (cross and circle) that are at the maximum margin (edge of margin width boundary) are called support vectors (SVs). SVs lie on the margin defining the hyperplane of maximum margin. The optimal separation of hyperplane refers to the decision boundary that minimizes misclassification obtained in the training step.³⁹ SVM assumes samples close to class boundary and work well with small training dataset quantity.⁴³ It uses a recursive procedure to generate prior probability estimation for known and unknown classes.³² Training dataset selection is supposed to describe each class in feature space in order to distinguish different class through training samples selection or support vectors that are closest to SVM hyperplane. The number of training examples in this study is less than 30 examples. SVs that do not contribute to the estimation of hyperplane location, are dropped which will be useful for an accurate classification of imagery.⁴²

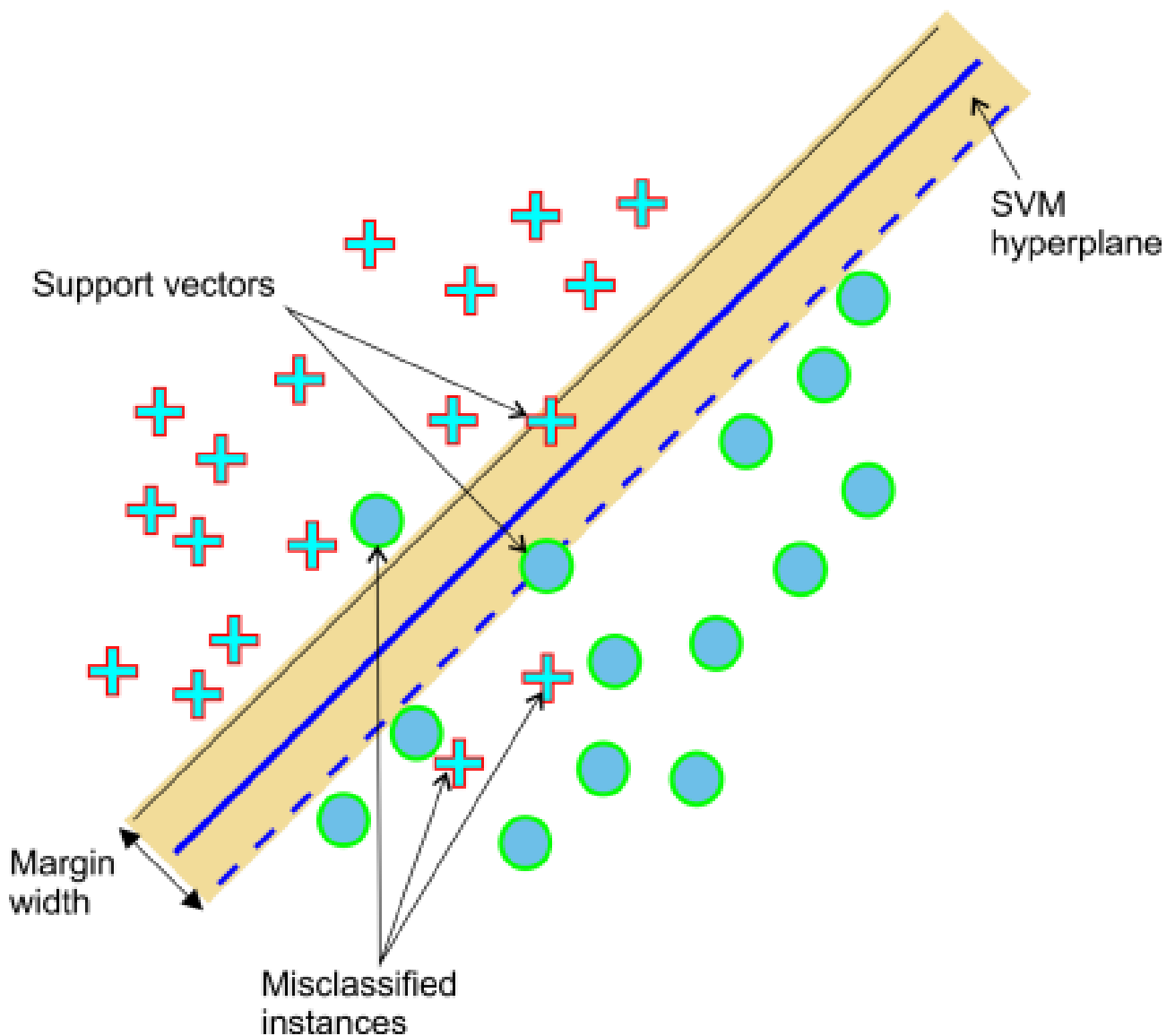


Figure 5: Scheme illustration of SVM

Results and Discussion

Multi-polarization: Figure 6 shows images generated from multi-polarization technique using median filter combination with kernels of 3x3 and 5x5. Figure 6 shows the sample of water area (non-flooded and flooded area) including river water, crops water and pond water. Multi-polarization image provides the clear information of flood water through its colour and pattern. Figure 6(a) shows areas of pre-flooding images in VH polarization presenting water in gray-black tones and colours. Figure 6(b) shows area samples of flooding images in multi-polarization presenting the clear display of land surface and the strong black colour of water.

Flood detection: Figure 7 shows some of image samples classified by thresholding, SVM and visual interpretation. It can be observed that the flood polygons generated from thresholding have the similarity to SVM. Figure 7(b) shows that the flooded area could be detected successfully using thresholding method by recognizing the dark-coloured pixels as water and the light-coloured pixels as non-water. Figure 7(c) shows that SVM is able to detect the flooded area in details although the presence of water is commonly unclear through human eyes. It can be seen that there are several flooded areas detected in the location that are hard to

be interpreted visually such as in the pond area. Figure 7(d) shows the flooded area map generated from visual interpretation using multi-polarization image.

Figure 8 shows the flooded area maps generated from SAR Sentinel-1A using three methods: (a) visual interpretation, (b) thresholding and (c) SVM and compared to the classification result obtained by visual interpretation using Planetscope-3A image (Figure 8d). Figures 8(b) and 8(c) show that results generated from thresholding and SVM methods are more similar to the flooded area generated from visual interpretation using Planetscope-3A image. This fact is confirmed by the total flooded area as shown in table 2. Table 2 shows the total flooded area in study area according to each method. Each method provides an area of 422.86 ha (visual interpretation), 791.22 ha (thresholding), 1084.76 ha (SVM) and 1001.52 ha (Planetscope-3A).

All methods have the similarity showing that floods dominate in river side and cultivated crop areas. However, the flooded area generated from visual interpretation method is very different from other methods. Figure 8(a) is showing that flooded areas generated by visual interpretation are not evenly distributed in study area. It may be due to the selection of classification features or training datasets between flood and non-flood water.

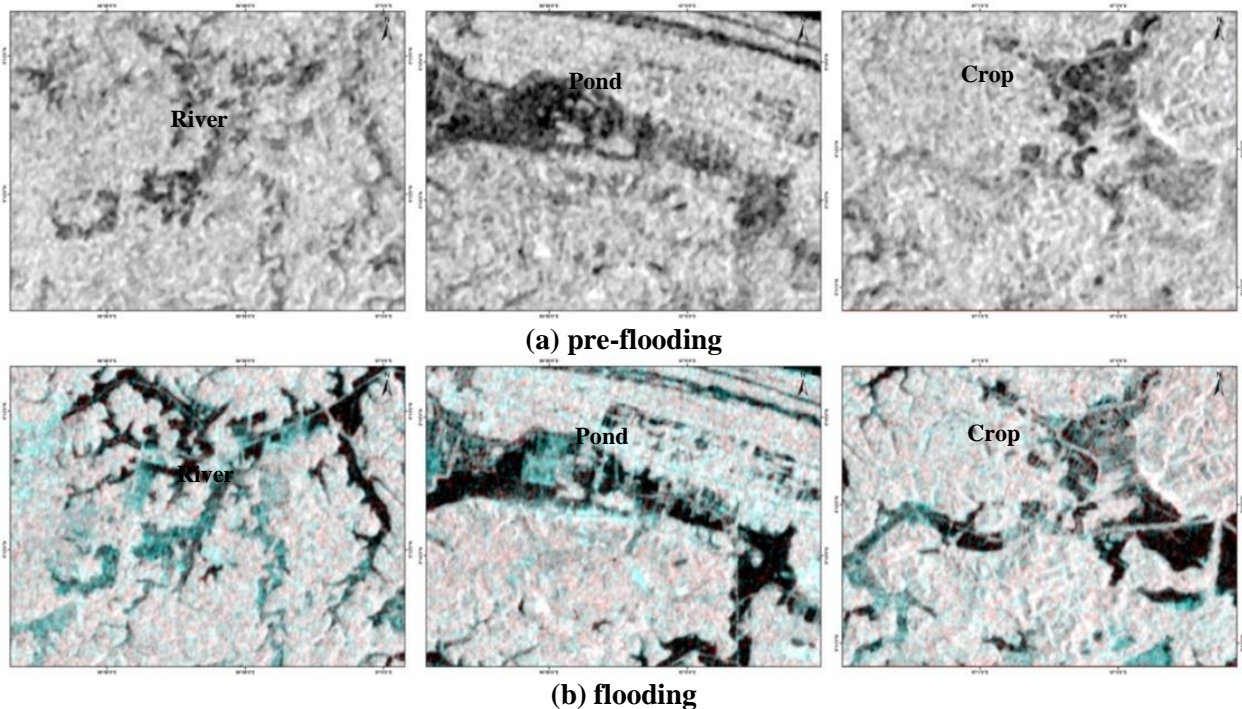


Figure 6: Images of pre-flooding and flooding in study area

**Table 2
Total flooded area of three methods used in this study**

Method	Flooded area (ha)
Visual interpretation	422.86
Thresholding	791.22
SVM	1084.76
Visual interpretation using Planetscope-3A	1001.52

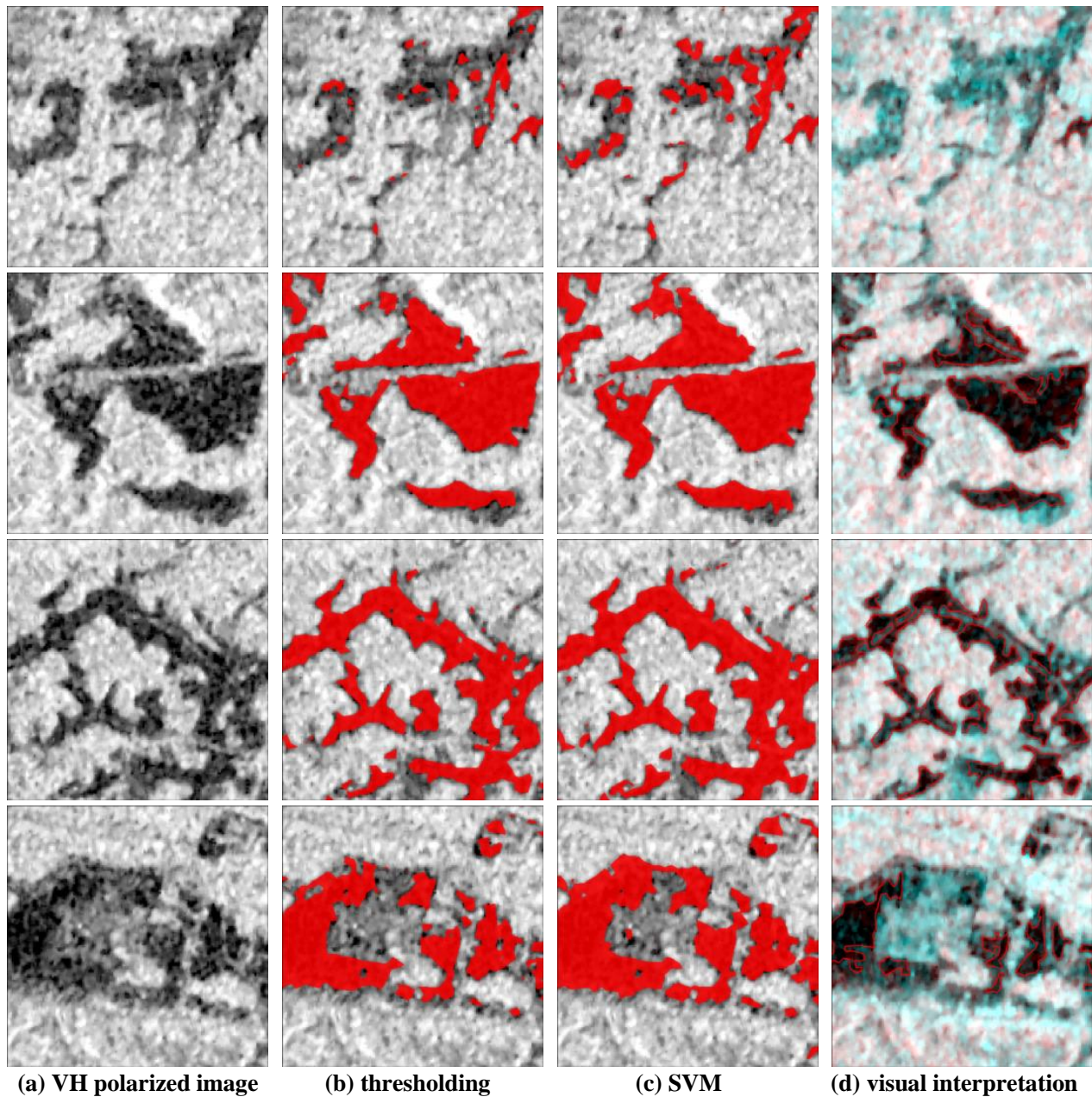


Figure 7: Results of flood detection

The problem of visual interpretation method is execution time. Using SAR Sentinel-1A image, delineating the water flood in the wide study area that has numerous heterogeneous surface features, takes more time. However, multi-polarized SAR Sentinel-1A image is very helpful in interpreting flood water relying on object, color, shape and pattern that can avoid the misclassification of flood water. This limitation can be solved by SVM and thresholding methods. SVM predicts flood water through the pixel value in image. Each pixel has the value representing each object based on a number of classes determined. However, SVM also has the limitations of flood objects misclassification which have the similar spectral response.

Regarding this limitation, there are two points that should be improved in SVM classification: increasing of the training sample size and improving of training sample distribution

representing each pixel value of flood water and non-flood water. Anyhow, it should be noted that the method of SVM is well-known by its small training datasets for classification. Thus, it should be adapted to the study area and object characteristics to classify.

Analysis of the impact of flooding on land cover: Figure 9(a) presents the land cover map covering the study area and figure 9(b) presents the land cover of study area affected by flood event using the flood data of SVM method.

Land cover consist of classes of water (4.69 km²/5.86 %), trees (15.84 km²/19.80 %), grass (0.66 km²/0.83 %), crops (31.67 km²/39.59 %), built area (27.01 km²/33.76 %) and barren land (0.13 km²/0.16 %). It shows that floods are distributed in each land cover with the different area.

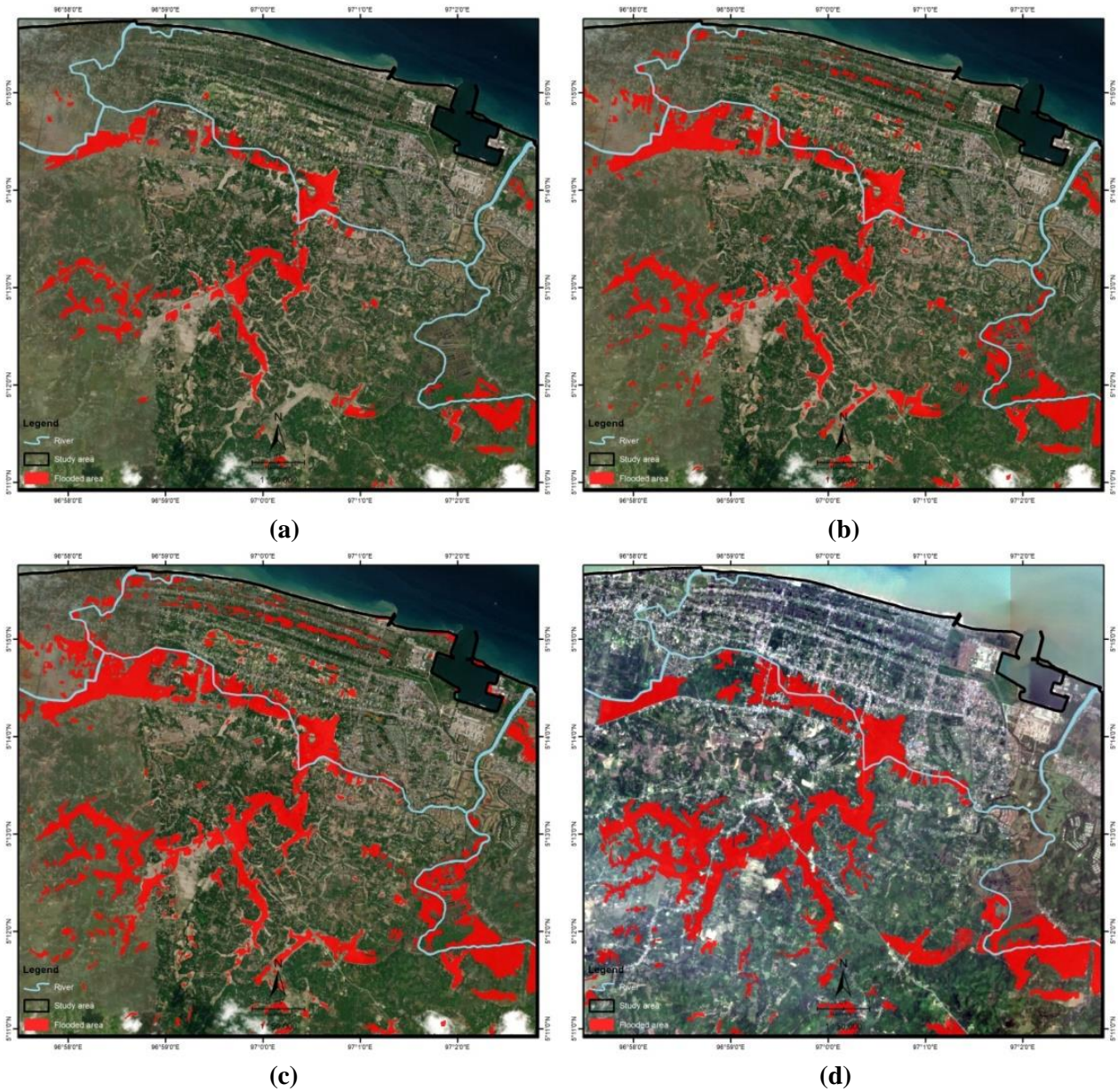


Figure 8: Flooded area maps

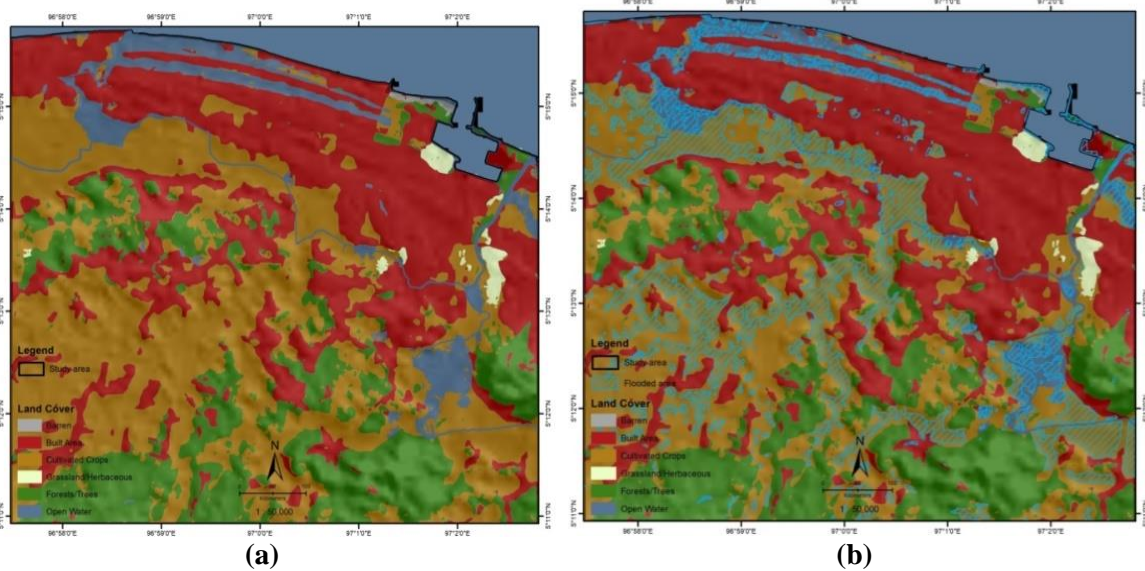


Figure 9: Maps of land cover in study area affected by flood

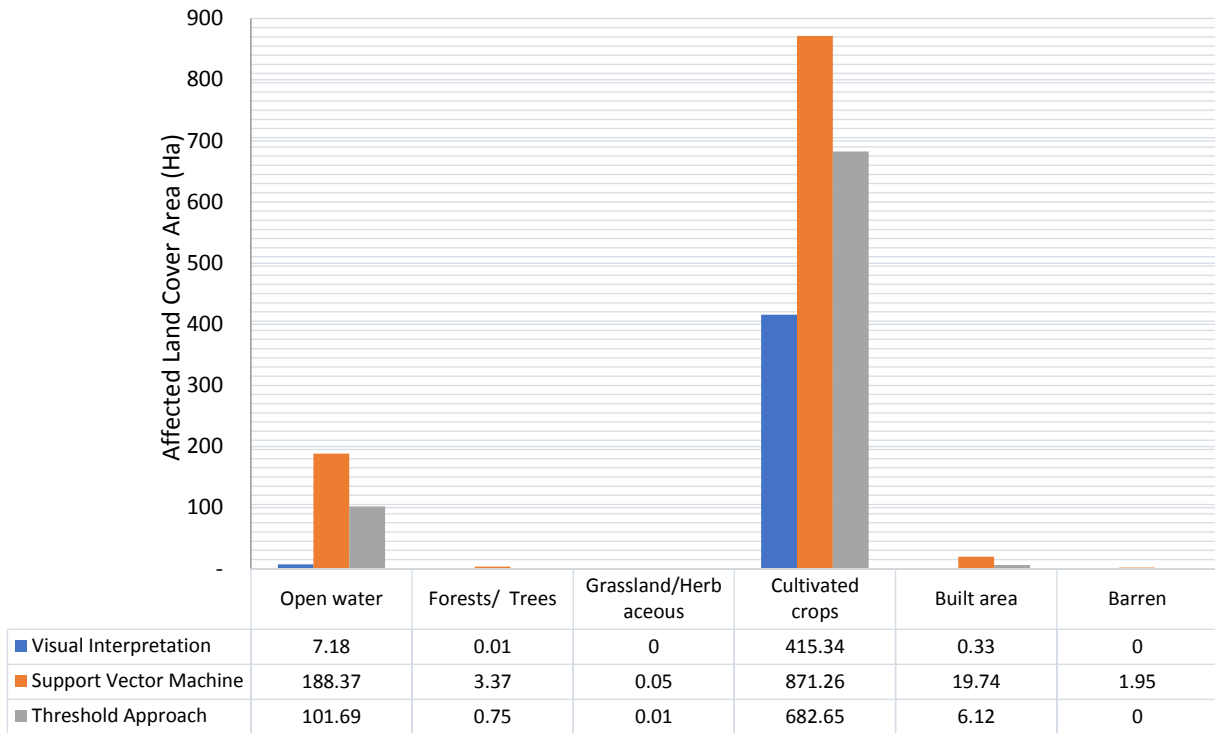


Figure 10: Graphic of flooding impact against land cover in study area

It can be seen that cultivated crop is the land cover affected so much by flood event. This fact is confirmed by the total flooded area as shown in graphic of figure 10 presenting the flooded area generated by each method. Each method shows that cultivated crop is the land cover mostly affected by flood. The total area of cultivated crops class inundated by the flood is 415.34 ha (visual interpretation), 682.65 ha (thresholding) and 871.26 ha (SVM). It is followed by water class with a total area of 7.18 ha (visual interpretation), 101.69 ha (thresholding) and 188.37 ha (SVM) and built area class with a total area of 0.33 ha (visual interpretation), 6.12 ha (thresholding) and 19.74 ha (SVM).

Figure 10 shows that classes of grassland/herbaceous and barren have very little flood area. These results cannot be said to be accurate because these results follow the available land cover. These problems can be solved through the use of recent land cover obtained from very-high resolution image that can be applied using advanced deep learning methods. It will absolutely provide the detailed results of land covers affected by flood event.

Conclusion

This study compared the variability of flood detection application using methods of visual interpretation, thresholding and SVM from SAR Sentinel-1A image data. The results indicate that the three methods are able to classify the flood water and detect the flooded areas. The key point of this study is to determine and provide the most effective method in detecting the flooded area. This study found that result generated by SVM method has the better accuracy when compared with the result generated by visual

interpretation method using high resolution image PlanetScope-3A.

More importantly, the results show that SAR Sentinel-1A image can become a data source used to detect rapidly the flooded area by flood detection methods. The flooded area maps generated from these methods are very helpful to assess the damage and loss of flood event and to map the flood prone areas. The future work shall deal with the application of Deep Learning for automatic flood detection that can be reference for urban planning management as a tool for flooded area mapping and alert systems in order to face the issues of climate change.

Acknowledgement

The authors are thankful to both European Space Agency (ESA) and Planet for freely providing Sentinel-1A and PlanetScope satellite images. This manuscript would not have been possible without the dataset made available by these institutions.

References

1. Aduah M., Maathuis B. and Ali H.Y., Synergistic use of optical and radar remote sensing for mapping and monitoring flooding system in Kafue flats wetland of southern Zambia, ISPRS Commission VII meeting (2007)
2. Angiati E., Dellepiane S., De Martino M., Moser G. and Serpico S.B., Flooding and change maps from COSMO-SKYMED images, Riunione Annuale GTTI (2010)
3. Boccoardo P. and Tonolo F.G., Advances in Mapping from Remote Sensor Imagery, Techniques and Applications, CRC Press, Boca Raton, 394–396 (2013)

4. Campbell J.B. and Wynne R.H., Introduction to Remote Sensing 5th edition, The Guilford Press, New York, 222–235 (2011)
5. Chini M., Hostache R., Giustarini L. and Matgen P., A Hierarchical Split-Based Approach for Parametric Thresholding of SAR Images: Flood Inundation as a Test Case, *IEEE Transactions on Geoscience and Remote Sensing*, **55**(12), 6975–6988 (2017)
6. Chini M., Pelich R., Pulvirenti L., Pierdicca N., Hostache R. and Matgen P., Sentinel-1 InSAR Coherence to Detect Floodwater in Urban Areas; Houston and Hurricane Harvey as A Test Case, *Remote Sensing*, doi: 10.3390/rs11020107, **11**(2), 1–20 (2019)
7. Chini M., Pulvirenti L. and Pierdicca N., Analysis and interpretation of the COSMO-SkyMed observations of the 2011 Japan tsunami, *IEEE Geoscience and Remote Sensing Letters*, doi: 10.1109/LGRS.2011.2182495, **9**(3), 467–471 (2012)
8. Corbley K., Remote Sensing and GIS provide rapid response for flood relief, *Ear. Obs. Mag*, 28–30 (1993)
9. Cristianini N. and Ricci E., Support Vector Machines in Encyclopedia of Algorithms, Springer, 928–932 (2008)
10. Cristianini N. and Shawe-Taylor J., An Introduction to Support Vector Machines and other kernel-based learning methods, Cambridge University Press, UK (2000)
11. Crystiana I., Hartono H., Jatmiko R.H. and Junaedi T., Multi-polarization for analysis of geological structures as formation of hydrocarbon traps controller in East Java basin, *Scientific Contributions Oil and Gas*, doi: 10.29017/SCOG.41.2. 335, **41**(2), 61–73 (2018)
12. Dasgupta A., Grimaldi S., Ramsankaran R., Pauwels V.R.N., Walker J.P., Chini M. and Matgen P., Flood Mapping Using Synthetic Aperture Radar Sensors From Local to Global Scales, *Geophysical Monograph Series*, doi: 10.1109/LGRS.2018.2871849, 55–77 (2018)
13. Dellepiane S.G. and Gemme L., Adaptive SAR Image Processing Techniques to Support Flood Monitoring from Earth Observation Data, *Springer Remote Sensing/Photogrammetry*, doi: 10.1007/978-3-319-63959-86, 115–134 (2017)
14. Dellepiane S., Angiati E. and Vernazza G., Processing and segmentation of COSMO-SkyMed images for flood monitoring, *IEEE International Geoscience and Remote Sensing Symposium*, doi: 10.1109/IGARSS.2010.5653960, 4807–4810 (2010)
15. Dewan A.M., Kankam-Yeboah K. and Nishigaki M., Using Synthetic Aperture Radar (SAR) Data for Mapping River Water Flooding in an Urban Landscape: A Case Study of Greater Dhaka, Bangladesh, *Journal of Japan Society of Hydrology and Water Resources*, doi: 10.3178/jjshwr.19.44, **19**(1), 44–54 (2006)
16. European Space Agency, <https://scihub.copernicus.eu/dhus/#/home> (Accessed 2022-10-03) (2022)
17. Galy H.M. and Sanders R.A., Using Synthetic Aperture Radar Imagery for Flood Modelling, *Trans. In GIS*, **6**(1), 31–42 (2002)
18. Ghapar A.A., Yusof S. and Bakar A.A., Internet of Things (IoT) architecture for flood data management, *International Journal of Future Generation Communication and Networking*, doi: 10.14257/ijfgcn.2018.11.1.06, **11**(1), 55–62 (2018)
19. Giustarini L., Hostache R., Matgen P., Schumann G.J.P., Bates P.D. and Mason D.C., A change detection approach to flood mapping in urban areas using TerraSAR-X, *IEEE Trans. Geosci. Remote Sens.*, doi: 10.1109/TGRS.2012.2210901, **51**(4), 2417–2430 (2013)
20. Glade T., Albini P. and Frances F., The use of historical data in natural hazard assessments Vol. 17 (An introduction), Kluwer Academic Publishers (2001)
21. Glago F.J., Flood Disaster Hazards; Causes, Impacts and Management: A State-of-the-Art Review, *IntechOpen*, doi: 10.4102/jamba.v11i1.789 (2021)
22. Glago F.J., Household disaster awareness and preparedness: A case study of flood hazards in Asamankese in the West Akim Municipality of Ghana, *Jàmbá: Journal of Disaster Risk Studies*, doi: 10.4102/jamba.v11i1.789, **11**(1), 1–11 (2019)
23. Guha A.K., Kumranchat V.M., Kamaraju M.V.V. and Govindha R.K.B., Potentials of Alternate Polarization of Envisat ASAR Data in Geological Mapping - A Case Study in Kurnool Group of Rocks andhra Pradesh, *Journal of the Geological Society of India*, doi: 10.1007/s12594-009-0083-z, **73**(2), 268–272 (2009)
24. Han D., Chan L. and Zhu N., Flood forecasting using support vector machines, *Journal of Hydroinformatics*, doi: 10.2166/hydro.2007.027, **9**(4), 267–276 (2007)
25. Handayani W., Chigbu U.E., Rudiarto I. and Putri H.S., Urbanization and Increasing Flood Risk in the Northern Coast of Central Java–Indonesia: An Assessment towards Better Land Use Policy and Flood Management, *Land*, doi: 10.3390/land9100343, **9**(10), 1–22 (2020)
26. Hong Y., Adhikari P. and Gourley J.J., Encyclopedia of Natural Hazards (Flood hazard and disaster), Springer, 326 (2013)
27. Hyndman D. and Hyndman D., Natural Hazards and Disasters 5th Edition, Cengage Learning, Boston, 381–384 (2014)
28. Inglada J. and Mercier G., A New Statistical Similarity Measure for Change Detection in Multitemporal SAR Images and Its Extension to Multiscale Change Analysis, *IEEE Transactions on Geoscience and Remote Sensing*, doi: 10.1109/TGRS.2007.893568, **45**(5), 1432–1445 (2007)
29. Li N., Wang R., Deng Y., Liu Y., Li B., Wang C. and Balz T., Unsupervised polarimetric synthetic aperture radar classification of large-scale landslides caused by Wenchuan earthquake in hue-saturation-intensity color space, *Journal of Applied Remote Sensing*, doi: 10.1117/1.JRS.8.083595, **8**(1) (2014)
30. Li Y., Martinis S., Wieland M., Schlaffer S. and Natsuaki R., Urban Flood Mapping using SAR Intensity and Interferometric Coherence via Bayesian Network Fusion, *Remote Sensing*, doi: 10.3390/rs11192231, **11**(9), 1–22 (2019)
31. Lillesand T.M., Kiefer R.W. and Chipman J.W., Remote Sensing and Image Interpretation 7th Edition, John Wiley and Sons, Inc, USA, 385–392 (2015)

32. Mantero P., Moser G. and Serpico S.B., Partially supervised classification of remote sensing images through SVM-based probability density estimation, *IEEE Transactions on Geoscience and Remote Sensing*, doi: 10.1109/TGRS.2004.842022, **43(3)**, 559–570 (2005)
33. Martinez J. and Letoan T., Mapping of flood dynamics and spatial distribution of vegetation in the Amazon floodplain using multitemporal SAR data, *Remote Sensing of Environment*, doi: 10.1016/j.rse.2006.11.012, **108(3)**, 209–223 (2007)
34. Mason D.C., Bevington J., Dance S.L., Revilla-Romero B., Smith R., Vetra-Carvalho S. and Cloke H.L., Improving Urban Flood Mapping by Merging Synthetic Aperture Radar-Derived Flood Footprints with Flood Hazard Maps, *Water*, doi: 10.3390/w13111577, **13(11)**, 1577 (2021)
35. Mason D.C., Dance S.L. and Cloke H.L., Floodwater detection in urban areas using Sentinel-1 and World DEM data, *Journal of Applied Remote Sensing*, doi: 10.1117/1.JRS.15.032003, **15(3)**, 032003-1–032003-22 (2020)
36. Mason D.C., Davenport I.J., Neal J.C., Schumann G.J.P. and Bates P.D., Near real-time flood detection in urban and rural areas using high-resolution synthetic aperture radar images, *IEEE Transactions on Geoscience and Remote Sensing*, doi: 10.1109/TGRS.2011.2178030, **50(8)**, 3041–3052 (2012)
37. Mason D.C., Speck R., Devereux B., Schuman G.J.P., Neal J.C. and Bates P.D., Flood detection in urban areas using Terrasar-X, *IEEE Transactions on Geoscience and Remote Sensing*, doi: 10.1109/TGRS.2009.2029236, **48(2)**, 882–894 (2010)
38. Merchant M.A., Adams J.R., Berg A.A., Baltzer J.L., Quinton W.L. and Chasmer L.E., Contributions of C-Band SAR Data and Polarimetric Decompositions to Subarctic Boreal Peatland Mapping, *IEEE Journal of Selected Topics in Applied Earth Observations and Remote Sensing*, doi: 10.1109/jstars.2016.2621043, **10(4)**, 1467–1482 (2017)
39. Mountrakis G., Im J. and Ogole C., Support vector machines in remote sensing: A review, *ISPRS Journal of Photogrammetry and Remote Sensing*, doi: 10.1016/j.isprsjprs.2010.11.001, **66(3)**, 247–259 (2011)
40. Oberstadler R., Honsch H. and Huth D., Assessment of the mapping capabilities of ERS-1 SAR data for flood mapping: A case study in Germany, *Hydrological Process*, doi:10.1002/(sici)1099-1085(199708)11:10<1415::aidhyp532>3.0.co;2-2, **11(10)**, 1415–1425 (1997)
41. Pulvirenti L., Chini M., Pierdicca N., Guerriero L. and Ferrazzoli P., Flood monitoring using multi-temporal COSMO-skymed data: image segmentation and signature interpretation, *Remote Sens. Environ.*, doi: 10.1016/j.rse.2010.12.002, **115(4)**, 990–1002 (2011)
42. Rokhmatuloh, Murfi H. and Tateishi R., Support Vector Machine (SVM) for classification of forest and non-forest derived from ALOS PALSAR Data, *Conference: ALOS Application and Verification Project in Indonesia*, doi: 10.13140/RG.2.1.1628.5041, 18–25 (2012)
43. Sambodo K.A. and Indriasari N., Land cover classification of ALOS PALSAR data using support vector machine, *International Journal of Remote Sensing and Earth Sciences*, **10(1)**, 9–18 (2013)
44. Schlaffer S., Chini M., Dettmering D. and Wagner W., Mapping wetlands in Zambia using seasonal backscatter signatures derived from ENVISAT ASAR time series, *Rem. Sens.*, doi: 10.3390/rs8050402, **8(5)**, 1–24 (2016)
45. Schumann G., Hostache R., Puech C. and Hoffmann L., High-resolution 3-D flood information from radar imagery for flood hazard management, *IEEE Transactions on Geoscience and Remote Sensing*, doi: 10.1109/TGRS.2006.888103, **45(6)**, 1715–1725 (2007)
46. Shi Y., Cheng T. and Taalab K.P., Flood Prediction using Support Vector Machines (SVM), *Proceeding of the 24th GIS Research UK (GISRUK) Conference* (2016)
47. Ustuner M., Sanli F.B. and Dixon B., Application of Support Vector Machines for Landuse Classification Using High-Resolution RapidEye Images: A Sensitivity Analysis, *European Journal of Remote Sensing*, doi: 10.5721/EuJRS20154823, **48(1)**, 403–422 (2015)
48. Vassileva M., Nascetti A., Tonolo F.G. and Boccoardo P., Unsupervised Flood Extent Detection from SAR Imagery Applying Shadow Filtering from SAR Simulated Image, *IEEE International Geoscience and Remote Sensing Symposium*, doi: 10.1109/IGARSS.2015.7326372 (2015)
49. Zehra N., Prediction Analysis of Floods Using Machine Learning Algorithms (NARX and SVM), *International Journal of Science: Basic and Applied Research*, **49(2)**, 24–34 (2020)
50. Zhang M., Chen F., Liang D., Tian B. and Yang A., Use of Sentinel-1 GRD SAR Images to Delineate Flood Extent in Pakistan, *Sustainability*, doi: 10.3390/su12145784, **12(14)**, 1–19 (2020)
51. Zhang W., Villarini G., Vecchi G.A. and Smith J.A., Urbanization exacerbated the rainfall and flooding caused by hurricane Harvey in Houston, *Nature*, doi: 10.1038/s41586-018-0676-z, 384–388 (2018)
52. Zhao M., Ling Q. and Li F., An Iterative Feedback-Based Change Detection Algorithm for Flood Mapping in SAR Images, *IEEE Geoscience and Remote Sensing Letters*, **16(2)**, 231–235 (2019).

(Received 11th September 2022, accepted 12th November 2022)